Intramolecular water divining: Locating H_2O inside a C_{60} cage

Samuel P Jarvis[1], Hongqian Sang[2,8], Filipe Junqueira[3], Oliver Gordon[3], Jo E. A. Hodgkinson[3], Alex Saywell[3], Philipp Rahe[4], Salvatore Mamone[3], Simon Taylor[3], Adam Sweetman[5], Jeremy Leaf[3], David Duncan[6], Tien-Lin Lee[6], Pardeep K. Thakur[6], Gabriella Hoffman[7], Richard Whitby[7], Malcolm Levitt[7], Georg Held[6], Lev Kantorovich[8], Philip Moriarty[3], and Robert G Jones[9]

[1] *Physics Department, Lancaster University, Lancaster, LA1 4YB, UK*

[2] *Institute for Interdisciplinary Research, Jianghan University, Wuhan 430056, China*

[3] *The School of Physics and Astronomy, The University of Nottingham, Nottingham NG7 2RD, UK*

[4] *Fachbereich Physik, Universität Osnabrück, Barbarastrasse 7, 49076 Osnabrck, Germany*

[5] *School of Physics and Astronomy, University of Leeds, Leeds, LS2 9JT, UK*

[6] *Diamond Light Source, Diamond House, Harwell Science & Innovation Campus, Didcot, Oxfordshire, OX11 0DE, UK*

[7] *School of Chemistry, The University of Southampton, Southampton, SO17 1BJ, UK*

[8] *Department of Physics, King's College London, The Strand, London, WC2R 2LS, UK and*

[9] *School of Chemistry, The University of Nottingham, Nottingham NG7 2RD, UK*

Abstract

We determine the location of an H_2O molecule isolated within an adsorbed buckminsterfullerene cage, and compare this to the intrafullerene position of HF. Using normal incidence X-ray standing wave (NIXSW) analysis, coupled with density functional theory and molecular dynamics simulations, we show that both H_2O and HF are located at an off-centre position within the fullerene cage, caused by substantial intra-cage electrostatic fields generated by surface adsorption of the fullerene. The atomistic and electronic structure simulations also reveal significant internal rotational motion consistent with the NIXSW data. Despite this substantial intra-cage interaction, we find that neither HF or H_2O contribute to the endofullerene frontier orbitals, confirming the chemical isolation of the encapsulated molecules. We also show that our experimental NIXSW measurements and theoretical data are best described by a mixed adsorption site model.

PACS numbers:

Keywords:

The extent to which trapped, encapsulated, or otherwise confined atoms and molecules are influenced by changes in the external electrostatic environment is a fascinating problem. Endohedral fullerenes[1–3] are an especially important molecular class from this perspective, with their properties exploited in areas as diverse as nanoelectronic components[4, 5], qubit candidates[6], and 'tracer' species or contrast agents[7, 8]. Of particular interest is the proposal that C_{60} acts as a Faraday cage[9–13], screening out electrostatic fields from its interior, and allowing near-complete decoupling of the encapsulated species from the outside world. The extent of electrostatic decoupling remains, however, very much an open question.

"Molecular surgery"[14] has provided exciting new opportunities to study much larger fullerene-encapsulated species than previously possible. One of the most well studied examples is $H_2O@C_{60}$[14–17], in which the encapsulated water molecule is free of any hydrogen-bonded partner. Ortho-para nuclear spin conversion has been observed in $H_2O@C_{60}$ by nuclear magnetic resonance (NMR)[18–20], infrared spectroscopy[16, 18], and pulsed terahertz spectroscopy[17]. Remarkably, ortho-para conversion has also been detected in this system by temperature-dependent capacitance measurements of bulk $H_2O@C_{60}$ crystals[21], strongly suggesting that, despite the shielding offered by the surrounding fullerene cage, the encapsulated water molecule can have a significant influence on the external environment. $HF@C_{60}$ has more recently been synthesised[22] and provides a key comparative system to that of $H_2O@C_{60}$, not least because of the strong similarity in the dipole moments of free H_2O and HF.

Hampered by the absence of clear experimental evidence, there has been considerable debate about the extent to which H_2O interacts with the C_{60} cage[4, 23–25]. Calculations of charge transfer result in a wide range of values[26]. Whilst some simulations suggest that the water molecule in $H_2O@C_{60}$ is electrostatically isolated[24], other reports suggest that the position and orientation of the encaspulated H_2O can be tuned via electric, magnetic or photon excitation[4], mechanical force[27], or static (or dynamic) fields[28].

Here we provide direct experimental measurement of the location of two separate encapsulated molecules, H_2O and HF, each caged within buckminsterfullerene, C_{60}, as illustrated in Figure 1 (a). Through single molecule scanning tunnelling microscopy, non-contact atomic force microscopy (ncAFM), and valence band photoemission, we show that the frontier orbital structure of the C_{60} molecule is unaffected by the presence of water inside the cage. Using the normal incidence X-ray standing wave (NIXSW) technique for the $H_2O@C_{60}$:Ag(111) system, we determine the intracage location of both H_2O and HF. The measured heights of the H_2O and HF molecules above the Ag(111) surface are in good agreement with dispersion-corrected density

functional theory (DFT) and molecular dynamics calculations, confirming the lack of chemical interaction of the encapsulated molecules with the surrounding carbon cage, yet revealing the strong influence of an adsorption-induced intra-fullerene electric field.

C_{60} as a Faraday cage? The local density of states of $H_2O@C_{60}$ was probed using STM measurements of a 70:30 mixture of empty and water-filled cages, deposited as a submonolayer on Cu(111). Analysis of C_{60} (sub)monolayers prepared at room temperature is complicated by the well-studied underlying surface reconstruction induced by fullerene adsorption[30]. Detailed low energy electron diffraction (LEED) studies by a number of groups have provided compelling evidence that fullerene-induced vacancy reconstruction is prevalent on Cu(111) and Ag(111) surfaces[31–33], with STM reports suggesting a mixed picture of "bright" and "dark" molecules[34, 35]. To confirm the presence of surface reconstruction, we compared STM measurements with constant height ncAFM imaging (figures 1(b) and 1(c)), which clearly reveals that the mixture of "bright" and "dark" features in figure 1(b) is indeed due to the variation of the geometric height of the adsorbed molecules. This most likely arises from a combination of atom-top and vacancy adsorption sites; the brightness variations observed in the STM image of figure 1(b) are unrelated to water encapsulation (see SI, figure S1).

Despite STM's exceptional sensitivity to minor changes in electronic structure, we found no difference between the appearance of empty and filled C_{60} molecules. This observation was confirmed across a wide range of different imaging parameters (figure S1), strongly suggesting that the frontier orbitals of the fullerene are unperturbed by the presence of H_2O. Similarly, ncAFM measurements, including force-distance analysis designed to compress individual fullerene cages, revealed no discernible differences (see Supplementary Information) above the noise floor of our measurements. These observations were further confirmed using valence band x-ray photoemission spectroscopy (VB-XPS) at the Diamond Light Source (Beamline I0-9) collected at a photon energy of 110 eV. VB-XPS of a bulk film of 95% pure $H_2O@C_{60}$ (thick enough to completely attenuate the Ag 3d core-level photoelectron peaks from the substrate) was indistinguishable from that of C_{60} within the limits of the natural, and substantial, linewidth broadening. There is no discernable difference between the spectrum shown in figure 1 (d) and that of empty C_{60}, acquired at the same photon energy (see, in particular, Ref.[29]). The lack of an oxygen contribution to the HOMO and HOMO+1 features was also verified via resonant photoemission at the O K edge (see SI, figure S2).

That STM, ncAFM, and photoemission spectroscopy (including resonant photoemission) are

each unable to distinguish between filled and empty C_{60} strongly suggests that neither electronic structure, the stiffness of the cage, nor the dielectric properties of the fullerene are appreciably affected by the presence of H_2O (somewhat at odds with other findings[21].) This seems to point towards a substantial screening of the encapsulate by the surrounding fullerene cage.

Locating trapped molecules with NIXSW. Given the inability of scanning probes and photoemission to distinguish between filled and empty fullerene cages, we turned to the normal incidence X-ray standing wave (NIXSW) technique[36–38], illustrated in Figure 2(a), to determine

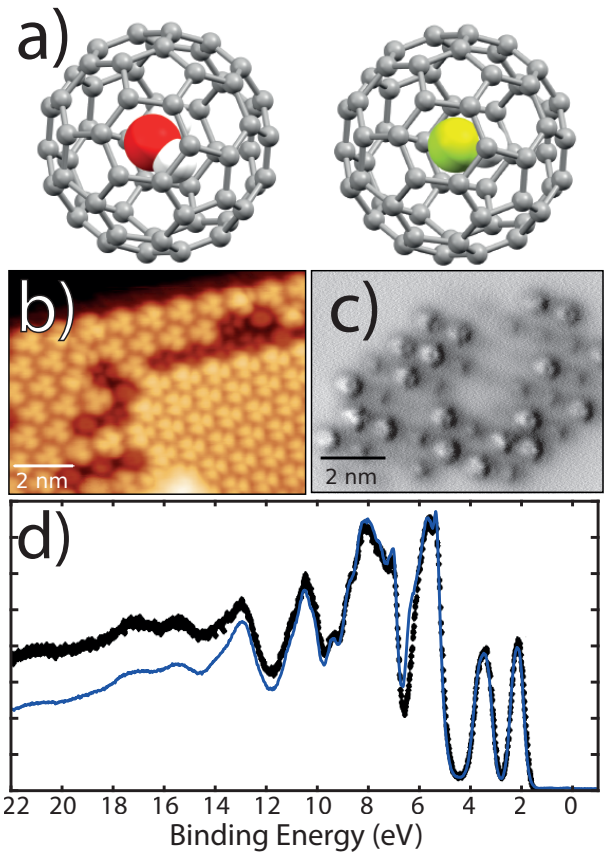

FIG. 1: **Endofullerene as a Faraday cage? (a)** Ball-and-stick models of $H_2O@C_{60}$ and $HF@C_{60}$. **(b)** STM image of a mixed (70:30) $H_2O@C_{60}$:C_{60} monolayer island on Cu(111) deposited at room temperature. The bright and dark molecules have a height difference of 200 pm resulting from the reconstruction of the underlying Cu(111) surface. **(c)** Constant height ncAFM image of a different island atop a reconstructed Cu(111) surface exhibiting clear variation in molecular height. **(d)** Valence band photoemission (synchrotron-based with $h\nu$ = 110eV) of a thick film of a 95% pure sample of $H_2O@C_{60}$ (blue line) shown with reference data for empty C_{60} (black line[29]). The scanning probe and photoemission data all point to a substantial screening of the encapsulated molecule. All SPM data were acquired at 5K. *Parameters*: (b) 1.5 V/ 10 pA; (c) Oscillation amplitude, a_0 =300 pm, $V = -2.1$ mV.

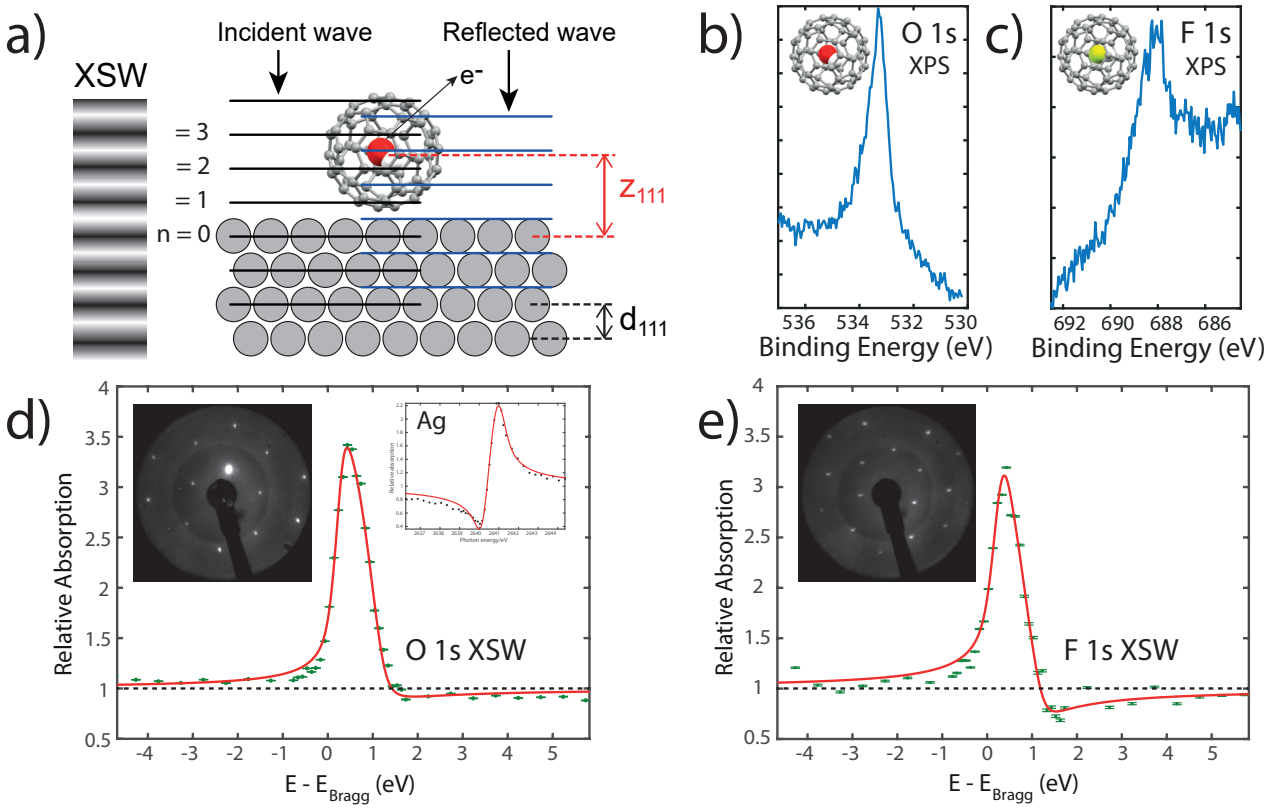

FIG. 2: **Locating trapped molecules with NIXSW. (a)** Diagram of the NIXSW technique; **(b)** O 1s core-level photoemission spectrum ($h\nu = 700$eV), and **(c)** F 1s level ($h\nu = 900$eV) for $H_2O@C_{60}$ and $HF@C_{60}$, respectively, both prepared as a single layer $(2\sqrt{3}$ x$2\sqrt{3})$R30° molecular superlattice on Ag(111). **(d)** NIXSW data for $H_2O@C_{60}$ with insets: bulk Ag NIXSW, and low energy electron diffraction (LEED, $E = 46.5eV$). $P_c = 0.35 \pm 0.03, F_c = 0.78 \pm 0.05$. **(e)** NIXSW data for $HF@C_{60}$. $P_c = 0.43 \pm 0.03, Fc = 0.72 \pm 0.07$, with inset LEED ($E = 50.5eV$). The NIXSW data were acquired at 20 K at the Ag{111} Bragg energy.

the intracage position of each encapsulated molecule. The location of H_2O was probed via the O 1s core-level photoelectron peak excited at the Ag{111} Bragg energy whereas HF was located using F 1s photoemission. Figures 2(b) and 2(c) show the O 1s and F 1s photoemission peaks acquired with a photon energy of 700 eV and 900 eV, respectively. (The lower photon energies, as compared to that used for the NIXSW measurements ($h\nu = 2637$eV at 20 K), were chosen to enhance the photoabsorption cross-section for high resolution photoemission measurements.)

Ag(111) was chosen as a substrate for these synchrotron-based measurements in order to exploit the well-defined $(2\sqrt{3}$ x $2\sqrt{3})$R30° molecular superlattice that forms on the silver surface[31, 39]. Results were collected at temperatures ranging from 20 K up to 200 K, with particular care taken to limit the degree of both extrinsic water adsorption at low temperatures and beam damage.

(See Supplementary Information.)

NIXSW results collected at 20 K for $H_2O@C_{60}$ and $HF@C_{60}$ are shown in Figure 2 (d) and (e), respectively. (See also figures S4 – S6 in the supplementary information file). The LEED patterns shown in the insets confirm the $(2\sqrt{3}$ x $2\sqrt{3})$R30° ordering of the molecular (sub)monolayer for both samples. The $H_2O@C_{60}$ XSW data averaged across the entire temperature range (see Fig. S6) are best fit using a coherent position, P_c, of 0.36±0.01 and a coherent fraction, F_c, of 0.72±0.06. (See reference[36] for a detailed explanation of the coherent position and coherent fraction parameters.) These measurements translate to an oxygen atom position, $z_{111}(O)$, of 5.57 ±0.03 Å above the Ag(111) surface. In comparison, and when again averaged across all temperatures, $HF@C_{60}$ results in a coherent position, P_c, of 0.40±0.05 and a coherent fraction, F_c, of 0.62±0.07, placing the fluorine atom at a position, $z_{111}(F) = 5.7 \pm 0.1$ Å above the Ag(111) surface. The uncertainties in z_{111} in each case are an upper limit, determined from repeated measurements across different temperatures and sample preparations. Our NIXSW measurements show that the H_2O and HF molecules are close to the centre of their respective fullerene enclosures.

Density functional theory and molecular dynamics. The results of the NIXSW measurements were compared to DFT calculations carried out within the VASP[40] framework, using DFT-D3[41] to account for dispersion forces. Calculations for a single C_{60} molecule were checked against a DFT-D3 simulation of the $(2\sqrt{3}$ x $2\sqrt{3})$R30° cell (Figure S10), where the adsorption heights were found to be almost identical. The remaining discussion therefore focusses on a single fullerene either adsorbed on an atom-top site or above a single-atom vacancy[31], both with a hexagonal face of the C_{60} cage aligned parallel to the surface.

Models of the DFT-D3-calculated geometries for $H_2O@C_{60}$ in the vacancy and atom-top arrangements are shown in Figure 3(a) and (b) (see Fig. S11 for $HF@C_{60}$). A key observation is that, on adsorption, there are significant offsets in the position of the internal molecule relative to the centre of the C_{60} cage. For $H_2O@C_{60}$ and $HF@C_{60}$ adsorbed in the vacancy site, the bottom layer of the C_{60} cage is calculated to be 1.89 Å above the surface Ag layer, resulting in a centre cage position of 5.17 Å. This is compared to an oxygen position of 5.03 Å, and a fluorine position of 5.24 Å, i.e. the oxygen atom is located 0.14 Å *closer* to the surface, whereas for HF the fluorine is located 0.07 Å *away* from the surface. Note that a detailed calculation of the potential energy surface of the frozen HF molecule inside the fixed C_{60} cage has also been reported[42] using the DF-MP2 method[43].

We find that the oxygen atom is located at 5.03 Å or 5.43 Å above the surface Ag(111) layer

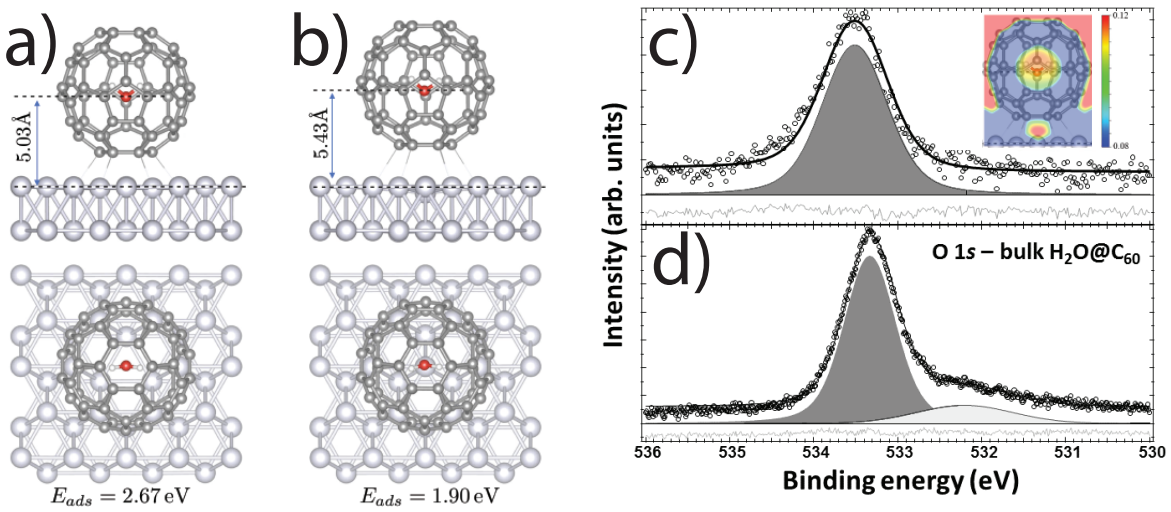

FIG. 3: **Dispersion corrected DFT of $H_2O@C_{60}$.** Ball-and-stick schematic showing DFT VASP results for $H_2O@C_{60}$:Ag(111) in **(a)** vacancy and **(b)** atom-top sites. The oxygen-Ag(111) separation is 5.03 Å and 5.43 Å, respectively. **(c)** and **(d)** show O 1s photoelectron spectra for the $H_2O@C_{60}$ monolayer and bulk film, respectively. Inset to **(c)** shows the DFT-predicted electric field distribution inside the cage. The broad additional peak in **(d)**, centred at approximately 532.2 eV, arises from contaminant material in the bulk film, and is removed in the monolayer sample during the additional 650 K anneal.

for the vacancy and atom-top structures, respectively – values that are both significantly different from that determined via the NIXSW measurements, i.e. 5.57 ± 0.03Å. A similar discrepancy between experiment and DFT calculations is observed for the $HF@C_{60}$ data: for example, DFT calculations (VASP) for the relaxed vacancy model predict a separation between the fluorine atom and the uppermost Ag(111) layer of 5.24 Å, as compared to the NIXSW measurement of 5.7 ± 0.1Å.

Calculated rotational energy barriers[44] for water in $H_2O@C_{60}$ are of the order of 8 meV – the encapsulated molecule is extremely mobile. We similarly found that molecular dynamics simulations (for T=180 K, and within the CP2K-DFT-D3 framework[45]) revealed significant internal rotational motion. Figure 4 (a) and (b) show plots of the internal molecular height and angle respectively, resulting in an average height increase of 0.3 Å relative to the ground state DFT calculation. This means that the average height is therefore 5.33 Å and 5.73 Å for the H_2O molecule in the vacancy and atop structures, respectively. (As discussed in the supplementary information, temperature-dependent NIXSW measurements showed little variation in the 20 K – 200 K range. See Fig. S6.)

Probing the intermolecular potential. The contribution of disorder notwithstanding, the

theoretically predicted intra-cage positions of the encapsulated H_2O and HF are due to charge redistribution from chemisorption of the C_{60} molecule on Ag(111)[46–48], producing an intracage electric field with which the internal molecules interact (Figure 3(c) inset). Good experimental evidence for the inhomogeneous electric field in $H_2O@C_{60}$ comes from O 1s photoelectron spectra. For a bulk endofullerene film, the O 1s peak associated with the encapsulated water has a Gaussian full width at half maximum of 0.7 eV, while for the chemisorbed monolayer the Gaussian width (under the same analyser operating conditions) increases almost 50% to 1.0 eV (compare Figure 3(c) and (d)). The O 1s peak position, as referenced to the Ag 3d core level binding energy, also shifts by approximately 200 meV. Given the lack of chemical interaction with the surrounding C_{60} cage, a plausible explanation for this 200 meV shift is that it arises from the difference in screening of the photogenerated core-hole due to the modification of the intracage electrostatic environment.

Moreover, molecular dynamics calculations semi-quantitatively explain the experimentally observed broadening of the O 1s photoemision peak and its shift to higher energies as compared to the bulk measurements. The O 1s core level shift (CLS) was approximately calculated[49] as the energy required to excite the O 1s core electron for a sampling of different geometries of the H_2O molecule inside the C_{60} cage obtained during the molecular dynamics simulations (see SI). We find that the full-width-at-half-maximum value of the distribution of the O 1s core-level shifts for the adsorbed $H_2O@C_{60}$ is indeed larger than that for the gas phase endofullerene, although the MD simulations produce a somewhat smaller increase in FWHM as compared to that seen in experiment (0.1 eV vs 0.3 eV.) Similarly, the O 1s binding energy determined via this calculation shifts towards higher energy, again in agreement with experiment, although the magnitude of the shift is overestimated as compared to the experimental value (0.20 eV vs 0.46 eV.) Considering the approximate character of the method used for the calculation[49], we would not expect full quantitative agreement. That the calculation reproduces both the direction of the shift in binding energy and the increase in broadening of the core-level peak seen in experiment provides good qualitative support for the presence and influence of the intra-cage electric field.

Mixed adsorption sites. As noted above, C_{60} adsorption on metal (111) substrates is a surprisingly complex problem, being highly surface dependent[30], and, as shown in Fig. 1(c), often associated with a significant inhomogeneity in molecular adsorption height. The majority of STM studies indicate a mixed picture[34, 35] of both "bright" and "dark" fullerenes (rather like those in figure 1(b)), where variations in brightness arise from a combination of atom-top and vacancy sites. In an influential piece of work, Li *et al.*[31] suggested that C_{60} molecules on

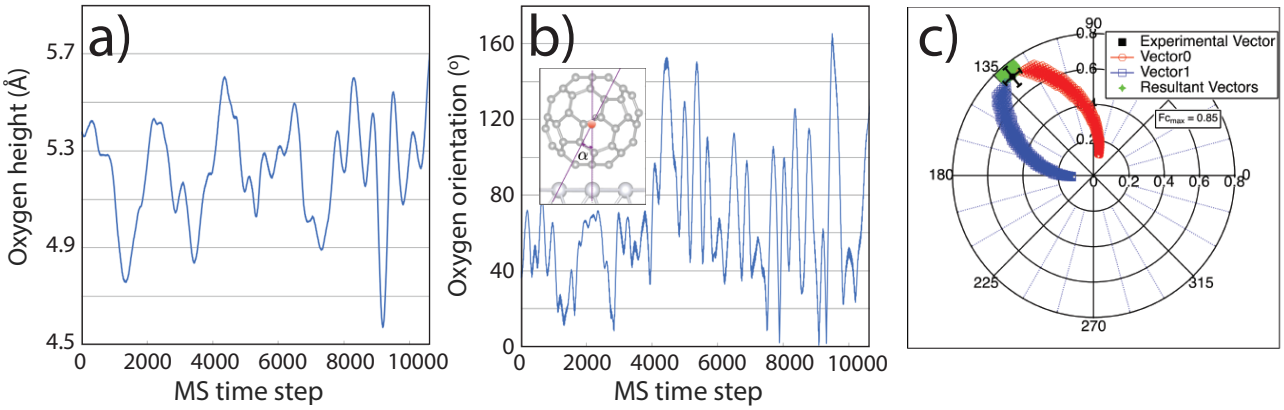

FIG. 4: **Dynamics and disorder in endohedral fullerenes.** Molecular dynamics simulations (T=180 K) showing **(a)** the height of the O atom of the intracage H_2O molecule above the Ag(111) surface, and **(b)** the angle between the H_2O C_2 axis and the vertical (as defined in the inset). **(c)** Average $F_c(T)$ (as radius length) and $P_c(T)$ (as angle) values for H_2O@C_{60} plotted on an Argand diagram, and their decomposition into two component vectors labelled 0 and 1.

Ag(111) situate in vacancy sites, evidenced by a compelling combined LEED and DFT study. In a follow-up report[33] the same authors extended this model, and determined that the ($2\sqrt{3}$ x $2\sqrt{3}$)R30° structure is in fact comprised of a mixture of C_{60} fullerenes on vacancy and atom-top sites. Indeed, our own LEED I(V) modelling (see Fig. S9 and associated discussion) using the DFT coordinates from figure 3, suggests that a mixture of the two adsorption sites is also highly likely in our system, giving rise to an appreciable amount of static disorder in the positions of the encapsulated molecules with respect to the Ag(111) substrate, and significantly complicating the XSW analysis.

To provide insight into whether the experimental NIXSW data are consistent with the mixed adsorption model we explored the parameter space via an Argand diagram analysis. In this approach, the experimental values for $F_c(T)$ and $P_c(T)$ are plotted as a vector, as shown in figure 4 (c). We decompose the experimental vector into two components, which we label 0 and 1, assigned to the vacancy and atom-top adsorption sites respectively. The vector combinations are then varied and recombined into a resultant (see SI for details) to represent different ratios of on-top and vacancy sites within the mixed film. A key difficulty in interpreting the NIXSW data in this way – and which we discuss in detail in the Supplementary Information – is that the underpinning equations are essentially under-determined and can therefore not be used to extract unique values of coherent fraction and coherent position. Despite this, the Argand analysis (summarised in figure 4(c) and detailed at length in the supplementary information file) illustrates

that the NIXSW data are broadly consistent with a mixture of on-top and vacancy adsorption sites, suggesting that the measured oxygen position of z_{111}(O), i.e. 5.57 ± 0.03 Å , can be interpreted as a combination of the two calculated positions of 5.33 Å and 5.73 Å for the H_2O molecule in the vacancy and atop structures, respectively.

In conclusion, our results address long-standing questions regarding the extent to which fullerene-encapsulated molecules, in particular H_2O, are electrostatically screened and decoupled from their external environment. Although both H_2O and HF contribute no discernable electronic state density to the frontier molecular orbitals of their surrounding C_{60} – in other words, there is a distinct lack of orbital mixing and hybridisation – adsorption on a metal surface (in this case, Ag(111)) causes a strong modification of the electrostatic potential within the cage. This in turn modifies the position of the encapsulated molecule as compared to that adopted in the gas phase endofullerene[4]. Direct determination of the position of the intracage molecule is, however, very much complicated by the bonding geometry of the parent fullerene; a naive interpretation of the XSW data by itself fails to capture the many subtle contributions to the intracage energy balance and dynamics. Instead, the results of a comprehensive series of DFT, MD, and XSW analyses of the position of the encapsulated H_2O and HF molecule can only be reconciled by taking into account both dynamic and static disorder in the position of the molecular encapsulate.

Methods

Scanning probe microscopy. Measurements were collected on a Createc GmbH LT STM-AFM system controlled by Nanonis electronics. Endohedral fullerenes were deposited via standard thermal sublimation under ultrahigh vacuum conditions (better than 1×10^{-10} mbar). For all SPM measurements we used a mixed monolayer film of C_{60}:H_2O@C_{60} (in a 70:30 ratio) on a clean sputter-annealed Cu(111) surface. For reconstructed samples the Cu(111) crystal was held at room temperature. For unreconstructed samples (See Supplementary Information, Fig. S1) the substrate was cooled to 77 K, followed by annealing to $\sim$ 200 K. A commercial qPlus sensor (Createc GmbH) with a separate tunnel current wire was used for both the STM and NC-AFM experiments ($f_0 \sim 20$ kHz; Q$\sim$30,000 at 5 K; nominal spring constant 1,800 Nm^{-1}).

Synchrotron XPS and NIXSW. Measurements were collected at beamline I09, Diamond Light Source. I09 is equipped with both a hard X-ray undulator, which was used for our XSW measurements at the Ag(111) Bragg energy of 2.63 keV, and a soft X-ray undulator, used for the acquisition of high resolution C 1s, O 1s, F 1s, and valence band spectra. All synchrotron data were collected on an Ag(111) crystal prepared by standard sputter-annealing methods, after which 95% pure samples of H_2O@C_{60} or HF@C_{60} were deposited via thermal sublimation. Considerable care was taken to reduce beam damage by detuning the beam and continuously moving

across the crystal (see Section I.1 of the Supplementary Information for more detail.)

DFT and MD calculations. Our relaxation calculations were based on density functional theory and were carried out using two *ab initio* codes: (i) the Vienna ab initio simulation package (VASP)[50] that uses plane waves basis set and norm-conserving pseudo-potentials, and (ii) the CP2K Quickstep package[45], which employs hybrid Gaussian and plane wave orbitals with a triple-zeta Gaussian molecularly optimized basis[51], and Goedecker-Teter-Hutter pseudopotentials[52]. In both sets of calculations the Perde-Burke-Ernzerhof (PBE) exchange-correlation density functional[53] was used and the dispersion interactions were added via the Grimme DFT-D3 method[54]. The geometry optimization was considered complete when the forces on atoms were better than 0.01 eVÅ. The Ag(111) surface was constructed using a slab model consisting of four atomic layers, where the atoms in the bottom two layers were kept fixed throughout all calculations. DFT simulations using VASP are regarded as being of higher precision due to the better approximation to a complete basis set that is possible with the inclusion of larger numbers of plane waves. Since MD simulations were, however, only possible using CP2K due to high computational cost, we have also provided in Fig. S11 CP2K results for two geometries of HF@C_{60} for validation purposes. MD simulations used a time step of 0.5 fs. Statistical analysis started from the 600th step, i.e. 0.3 ps after the NVT heat bath was applied. The temperature for MD was 180 K.

[1] X. Lu, L. Bao, T. Akasaka, and S. Nagase, Chem. Comm. **50**, 14701 (2014).

[2] X. Lu, L. Feng, T. Akasaka, and S. Nagase, Chem. Soc. Rev. **41**, 7723 (2012).

[3] A. Rodriguez-Fortea, A. L. Balch, and J. M. Poblet, Chem. Soc. Rev. **40**, 3551 (2011).

[4] C. Zhu and X. Wang, Sci. Rep. **5**, 17932 (2015).

[5] C. Joachim and J. Gimzewski, Chem. Phys. Lett. **265**, 353 (1997).

[6] W. Harneit, in *Endohedral fullerenes: Electron transfer and spin*, edited by A. Popov (2017), Nanostructure Science and Technology, pp. 297–324.

[7] R. D. Bolskar, Nanomedicine **3**, 201 (2008).

[8] J. Zhang, Y. Ye, Y. Chen, C. Pregot, T. Li, S. Balasubramaniam, D. B. Hobart, Y. Zhang, S. Wi, R. M. Davis, et al., J. Am. Chem. Soc. **136**, 2630 (2014).

[9] P. Delaney and J. Greer, Appl. Phys. Lett. **84**, 431 (2004).

[10] M. N. Chaur, F. Melin, A. L. Ortiz, and L. Echegoyen, Ang. Chem. Int. Ed. **48**, 7514 (2009).

[11] S. Guha and K. Nakamoto, Coord. Chem. Rev. **249**, 1111 (2005).

[12] H. Shinohara, Rep. Prog. Phys. **63**, 843 (2000).

[13] Y. Rubin, in *Fullerenes and Related Structures* (1999), vol. 199 of *Top. Curr. Chem.*, pp. 67–91.

[14] K. Kurotobi and Y. Murata, Science **333**, 613 (2011).

[15] A. Krachmalnicoff, M. H. Levitt, and R. J. Whitby, Chem. Commun. **50**, 13037 (2014).

[16] A. Shugai, U. Nagel, Y. Murata, Y. Li, S. Mamone, A. Krachmalnicoff, S. Alom, R. J. Whitby, M. H. Levitt, and T. Room, *Infrared spectroscopy of endohedral water in* c_{60} (2021), 2102.06389.

[17] S. S. Zhukov, V. Balos, G. Hoffman, S. Alom, M. Belyanchikov, M. Nebioglu, S. Roh, A. Pronin, G. R. Bacanu, P. Abramov, et al., Scientific Reports **10** (2020).

[18] C. Beduz, M. Carravetta, J. Y.-C. Chen, M. Concistrè, M. Denning, M. Frunzi, A. J. Horsewill, O. G. Johannessen, R. Lawler, X. Lei, et al., Proc. Nat. Acad. Sci. **109**, 12894 (2012).

[19] S. Mamone, M. Concistr, E. Carignani, B. Meier, A. Krachmalnicoff, O. G. Johannessen, X. Lei, Y. Li, M. Denning, M. Carravetta, et al., The Journal of Chemical Physics **140**, 194306 (2014).

[20] B. Meier, K. Kouřil, C. Bengs, H. Kouřilová, T. C. Barker, S. J. Elliott, S. Alom, R. J. Whitby, and M. H. Levitt, Phys. Rev. Lett. **120**, 266001 (2018).

[21] B. Meier, S. Mamone, M. Concistre, J. Alonso-Valdesueiro, A. Krachmalnicoff, R. J. Whitby, and M. H. Levitt, Nature Comms. **6** (2015).

[22] A. Krachmalnicoff, R. Bounds, S. Mamone, S. Alom, M. Concistr, B. Meier, K. Kouil, M. E. Light, M. R. Johnson, S. Rols, et al., Nature Chem. **8**, 953 (2016).

[23] J. L. Dunn and E. Rashed, J. Phys.: Conf. Ser. **1148**, 012003 (2018).

[24] S. Kaneko, Y. Hashikawa, S. Fujii, Y. Murata, and M. Kiguchi, Chem. Phys. Chem. **18**, 1229 (2017).

[25] C. Zhu and X. Wang, J. Phys. Cond. Matt. **27** (2015).

[26] V. A and V. PR, Chem. Eur. J. **18**, 15345 (2012).

[27] K. Min, A. B. Farimani, and N. R. Aluru, Appl. Phys. Lett. **103** (2013).

[28] B. Xu and X. Chen, Phys. Rev. Lett. **110** (2013).

[29] P. Brühwiler, A. Maxwell, A. Nilsson, N. Martensson, and O. Gunnarsson, Phys. Rev. B **48**, 18296 (1993).

[30] J. Ledieu, milie Gaudry, V. Fourne, J. A. Smerdon, and R. D. Diehl, Zeitschrift fr Kristallographie - Crystalline Materials **232**, 629 (2017).

[31] H. I. Li, K. Pussi, K. J. Hanna, L. L. Wang, D. D. Johnson, H. P. Cheng, H. Shin, S. Curtarolo, W. Moritz, J. A. Smerdon, et al., Phys. Rev. Lett. **103** (2009).

[32] W. W. Pai, H. T. Jeng, C. M. Cheng, C. H. Lin, X. Xiao, A. Zhao, X. Zhang, G. Xu, X. Q. Shi, M. A. Van Hove, et al., Phys. Rev. Lett. **104** (2010).

[33] K. Pussi, H. I. Li, H. Shin, L. N. Serkovic Loli, A. K. Shukla, J. Ledieu, V. Fournée, L. L. Wang, S. Y. Su, K. E. Marino, et al., Phys. Rev. B **86**, 205406 (2012).

[34] E. I. Altman and R. J. Colton, Phys. Rev. B **48**, 18244 (1993).

[35] J. A. Gardener, G. A. D. Briggs, and M. R. Castell, Phys. Rev. B **80**, 235434 (2009).

[36] D. Woodruff, Rep. Prog. Phys. **68**, 743 (2005).

[37] R. Jones, A. Chan, M. Roper, M. Skegg, I. Shuttleworth, C. Fisher, G. Jackson, J. Lee, D. Woodruff, N. Singh, et al., J. Phys. Cond. Matt. **14**, 4059 (2002).

[38] J. Zegenhagen, Surf. Sci. Rep. **18**, 199 (1993).

[39] K. Pussi, H. I. Li, H. Shin, L. N. S. Loli, A. K. Shukla, J. Ledieu, V. Fournee, L. L. Wang, S. Y. Su, K. E. Marino, et al., Phys, Rev. B **86** (2012).

[40] J. Hafner, J. Comp. Chem. **29** (2008).

[41] S. Grimme, J. Antony, S. Ehrlich, and H. Krieg, J. Chem. Phys. **132** (2010).

[42] Y. N. Kalugina and P.-N. Roy, The Journal of Chemical Physics **147**, 244303 (2017).

[43] H.-J. Werner, F. R. Manby, and P. J. Knowles, The Journal of Chemical Physics **118**, 8149 (2003).

[44] A. B. Farimani, Y. Wu, and N. R. Aluru, Phys. Chem. Chem. Phys. **15**, 17993 (2013).

[45] J. Hutter, M. Iannuzzi, F. Schiffmann, and J. VandeVondele, Wiley Interdisc. Rev. Comp. Mol. Sci. **4**, 15 (2014).

[46] L. Tjeng, R. Hesper, A. Heessels, A. Heeres, H. Jonkman, and G. Sawatzky, Sol. St. Comm. **103**, 31 (1997).

[47] W. Yang, V. Brouet, X. Zhou, H. Choi, S. Louie, M. Cohen, S. Kellar, P. Bogdanov, A. Lanzara, A. Goldoni, et al., Science **300**, 303 (2003).

[48] A. J. Gibson, R. H. Temperton, K. Handrup, and J. N. O'Shea, Surf. Sci. **657**, 69 (2017).

[49] L. Köhler and G. Kresse, Phys. Rev. B **70**, 165405 (2004).

[50] G. Kresse and J. Furthmüller, Phys. Rev. B **54**, 11169 (1996).

[51] J. VandeVondele and J. Hutter, J. Chem. Phys. **127**, 114105 (2007).

[52] C. Hartwigsen, S. Goedecker, and J. Hutter, Phys. Rev. B **58**, 3641 (1998).

[53] J. P. Perdew, K. Burke, and M. Ernzerhof, Phys. Rev. Lett. **77**, 3865 (1996).

[54] S. Grimme, J. Antony, S. Ehrlich, and H. Krieg, J. Chem. Phys. **132**, 154104 (2010).